IOP-Induced Lamina Cribrosa Displacement and Scleral Canal Expansion: An Analysis of Factor Interactions Using Parameterized Eye-Specific Models

Ian A. Sigal,[1,2,3] *Hongli Yang,*[1,2,4] *Michael D. Roberts,*[2] *Claude F. Burgoyne,*[4] *and J. Crawford Downs*[2]

Purpose. To study the anterior–posterior lamina cribrosa deformation (LCD) and the scleral canal expansion (SCE) produced by an increase in IOP and identify the main factors and interactions that determine these responses in the monkey.

Methods. Eye-specific baseline models of the LC and sclera of both eyes of three normal monkeys were constructed. Morphing techniques were used to generate 888 models with controlled variations in LC thickness, position and modulus (stiffness), scleral thickness and modulus, and scleral canal size and eccentricity. Finite element modeling was used to simulate an increase in IOP from 10 to 15 mm Hg. A two-level, full-factorial experimental design was used to select factor combinations and to determine the sensitivity of LCD and SCE to the eight factors, independently and in interaction.

Results. LCD was between 53.6 μm (posteriorly) and −12.9 μm (anteriorly), whereas SCE was between 0.5 and 15.2 μm (all expansions). LCD was most sensitive to laminar modulus and position (24% and 21% of the variance in LCD, respectively), whereas SCE was most sensitive to scleral modulus and thickness (46% and 36% of the variance in SCE, respectively). There were also strong interactions between factors (35% and 7% of the variance in LCD and SCE, respectively).

Conclusions. IOP-related LCD and SCE result from a complex combination of factors, including geometry and material properties of the LC and sclera. This work lays the foundation for interpreting the range of individual sensitivities to IOP and illustrates that predicting individual ONH response to IOP will require the measurement of multiple factors. (*Invest Ophthalmol Vis Sci.* 2011;52:1896–1907) DOI:10.1167/iovs.10-5500

Lowering intraocular pressure (IOP) remains the only proven method of preventing or delaying the onset and progression of glaucomatous vision loss, yet the role of IOP in the neuropathy remains unclear.[1–3] Several studies have explored the hypothesis that an altered biomechanical environment within the optic nerve head (ONH), and the lamina cribrosa (LC) in particular, may contribute to disruption of the retinal ganglion cell axons and the subsequent loss of vision associated with glaucoma.[1,4–15] Hence, there has been a search for an association between changes in IOP and deformations of the LC.[5,8–13,16]

For some time the conventional paradigm was that, as IOP increases, the LC deforms posteriorly, with the sclera remaining essentially undeformed.[16,17] Results from initial studies using radiographic[10,11] or histologic[8,9] techniques, or measurements of the optic disc surface[15,18–20] were interpreted as supportive of this paradigm. More recent numerical[6,7,12,13,21–23] and experimental[24,25] studies, however, suggest that the relationship between IOP and the deformations of the LC and sclera are more complex than initially thought. It is now clear, for example, that as IOP varies, the sclera deforms, sometimes substantially, and that these deformations, when transmitted to the ONH, may play an important role in the response of the LC to IOP.[5,24–26] Numerical models have also predicted that IOP-related anterior–posterior displacements of the LC may be small and could be even smaller in magnitude than lateral LC displacements (i.e., in the plane of the sclera).[6,12,22,26,27] This is consistent with recent measurements obtained using 3D histomorphometry and optical coherence tomography (Burgoyne CF, et al. *IOVS* 2008;49:ARVO E-Abstract 3655; Agoumi Y, et al. *IOVS* 2009;50:ARVO E-Abstract 4898).[25,28] It is now generally accepted that the LC does not respond to IOP changes in isolation, but rather that the ONH and peripapillary sclera behave as a mechanical system, and that the IOP-related deformations of the lamina and sclera are linked. Still, it is not clear how the LC and sclera deform as IOP changes, or how these deformations depend on the tissues' geometry and material properties. Numerical studies suggest that proper characterization of ONH biomechanics requires considering factor interactions (i.e., that the influence of one factor depends on the level of another). Although this seems reasonable, to the best of our knowledge, the role of factor interactions on LC and sclera deformations has not been reported.

The broad objective of this work was to study IOP-related anterior–posterior LC displacement (LCD) and scleral canal expansion (SCE). Specifically, we used newly developed parameterized eye-specific finite element models of normal monkey eyes to determine how LCD and SCE depend on the geometry and mechanical properties of the lamina and sclera. We identify the most influential factors, or parameters, and the interactions between them. This work also complements previous numerical and experimental studies by extending to the analysis of IOP-induced LCD and SCE the bioengineering and statistical techniques that we have applied to stresses and strains.[5,21]

From the [1]Department of Biomedical Engineering, Tulane University, New Orleans, Louisiana; and the [2]Ocular Biomechanics and [4]Optic Nerve Head Research Laboratories, Devers Eye Institute, Portland, Oregon.

[3]Present affiliation: Department of Ophthalmology, University of Pittsburgh, Pittsburgh, Pennsylvania.

Supported by National Institutes of Health Grants R01-EY18926 (JCD), R01-EY19333 (JCD), and R01-EY11610 (CFB) and the Legacy Good Samaritan Foundation, Portland, OR.

Submitted for publication March 9, 2010; revised July 9, 2010; accepted September 6, 2010.

Disclosure: **I.A. Sigal**, None; **H. Yang**, None; **M.D. Roberts**, None; **C.F. Burgoyne**, None; **J.C. Downs**, None

Corresponding author: J. Crawford Downs, Ocular Biomechanics Laboratory, Devers Eye Institute, 1225 NE Second Avenue, Portland, OR 97232; cdowns@deverseye.org.

METHODS

Our general strategy was as follows: we constructed eye-specific baseline models of the lamina and sclera of both eyes of three normal monkeys 2 to 10 years old. The geometry and material properties of each baseline model were parameterized by using morphing techniques.[29,30] This enabled us to produce new "morphed" models related to the baseline with precisely controlled variations in geometry and materials by specifying a few high-level parameters or factors. We produced six families of models, one per baseline model, spanning the physiologic ranges of the factors following a design of experiments statistical approach.[31,32] Eight factors were studied: seven parameterized factors (five geometric and two material) and the baseline model. Each model was solved using finite element techniques to predict the LCD and SCE resulting from an increase in IOP. The process was repeated for all six eye-specific models. We then used factor analysis techniques to determine the sensitivity of LCD and SCE to the factors and factor interactions. Preprocessing, including morphing and meshing, and postprocessing were done using Python scripts (www.Python.org/ open-source software provided by the Python Software Foundation) and a combination of standard and custom modules in commercial software (Amira; ver. dev4.1.1; Visage Imaging, Richmond, VIC, Australia); finite element analysis and statistical design and analysis were also performed with commercial software (Abaqus, ver. 6.8.1; Dassault Systèmes, Vèlizy-Villacoublay, France; and Design-Expert, ver. 7; Stat-Ease, Minneapolis, MN, respectively).

The Baseline Model Geometries

All animals were treated in accordance with the ARVO Statement for the Use of Animals in Ophthalmic and Vision Research. The eyes have been used in other studies by our group, for morphometry,[24,33,34] to characterize the LC microarchitecture,[35] and in analyses of the stresses and strains within the LC induced by an acute increase in IOP (Kodiyalam S, et al. *IOVS* 2009;50:ARVO E-Abstract 4893.[12,36] These studies provide the details of tissue preparation and 3D reconstruction of the ONH geometry in a way suitable for finite element modeling. Briefly, the eyes were perfusion fixed at an IOP of 10 mm Hg. The ONH and peripapillary sclera were trephinated (6-mm diameter) and embedded in paraffin. A microtome-based serial sectioning technique was used to acquire consecutive stained block-face images. The images were aligned and assembled into a stack (voxel resolution, 1.5 × 1.5 × 1.5 μm). The neural canal wall and the anterior and posterior surfaces of the LC and peripapillary sclera were manually delineated in custom software. The delineations were then used to construct smooth triangulated surfaces representing the eye-specific geometry of the LC and peripapillary sclera, which were then integrated into a generic shell with anatomic shape and thickness (Fig. 1).

Parameterizing the Geometry

Five features of the model geometry were defined (Fig. 1): scleral canal size and eccentricity, LC position and thickness, and scleral thickness. Lamina position represents the depth of the lamina anterior surface with respect to its periphery. Defined in this way, lamina position is independent of canal size, which simplifies the analysis of factor interactions.[31,32] Scleral canal eccentricity represents the shape of the canal, similar to the ovality used for the optic disc,[37] and was defined as the ratio of the major to minor axes of the anterior lamina insertion. The five features were parameterized using morphing techniques, which are described and discussed in detail elsewhere.[29] Scleral canal size and eccentricity were parameterized based on the distance to the centroid of the scleral canal opening. Deformations with the same sign along the major and minor axes of the canal opening resulted in expansions and contractions of the canal that preserved canal eccentricity, whereas deformations with opposite signs varied the eccentricity and preserved canal size. LC thickness and position were parameterized based on vectors normal to the anterior and posterior lamina surface. Deformations of both anterior and posterior lamina surfaces together varied lamina position and preserved thickness, whereas deformations of only the posterior lamina surface varied lamina thickness and preserved position. Scleral thickness was parameterized as described in our previous report.[29] In addition to the five geometric features described above, we also studied intereye variability by defining eye as a nominal categorical factor with six levels.

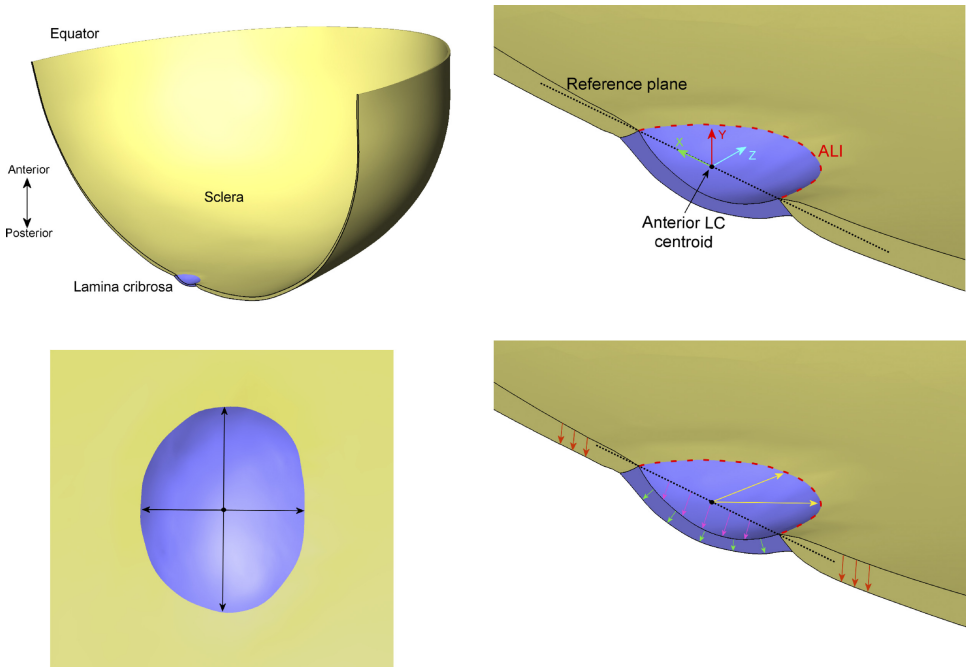

FIGURE 1. Geometry factor definitions. *Top left*: cutaway view of a baseline eye-specific model of a normal monkey eye, with the lamina in *blue* and the sclera in *yellow*. *Top right*: detail of the optic nerve head (ONH) region illustrating the location and orientation of the LC relative to the coordinate's origin. The model was translated and rotated so that the centroid of the anterior lamina insertion was located at the coordinate's origin. Also shown are the anterior lamina insertions into the sclera (ALI, *dashed red line*), a least-squares, best-fit reference plane to the ALI (*dotted black line*). Five features of the model geometry were defined. *Bottom left*: canal eccentricity as the ratio of the major to minor axes of the anterior lamina insertion; *bottom right*: canal size as the average canal radius, itself computed as the distance from the anterior lamina insertion to its centroid (*yellow arrows*); LC thickness, as the average distance between the anterior and posterior surfaces of the LC (*green arrows*); scleral thickness, as the distance between the interior and exterior surfaces of the sclera averaged over the sclera region located between 1.5 and 1.6 times the canal radius from the anterior lamina insertion centroid (*red arrows*); and LC position, as the average distance between the anterior surface of the lamina and a least-squares, best-fit plane to the anterior lamina insertion (*pink arrows*).

TABLE 1. Factors Studied and Their Levels

	Factor	Factor Range Low	Factor Range High
Geometry	Scleral canal size (radius), μm	569	787
	Scleral canal eccentricity	1.24	1.57
	Sclera thickness, μm	116	217
	Lamina cribrosa thickness, μm	82	150
	Lamina cribrosa position, μm	42	152
Mechanical properties	Sclera modulus, MPa	5.3	18.4
	Lamina cribrosa modulus, MPa	0.39	3.7
Eye	Nominal categorical factor with six levels		

See Figures 1 and 2 for the geometry definitions and ranges, respectively.

The ranges over which the geometric factors were varied were obtained from 3D histomorphometry of 21 normal monkey eyes[24,25,28,33,34,38] and are listed in Table 1 and illustrated in Figure 2.

Parameterizing the Mechanical Properties

All tissues were assumed to be linearly elastic, isotropic, and homogeneous, and therefore their mechanical behavior is determined by their Young's moduli, which we parameterized, and their Poisson ratio, which we kept constant at 0.45, close to the incompressible limit of 0.5 (Table 1). Several strategies were considered for selecting the ranges of material properties. For the scleral modulus we considered a range based on the literature,[5,39] based on the equilibrium moduli reported by Downs et al.[40] from uniaxial tests or based on averages of C_{1111} and C_{2222} at 10 mm Hg for young and adult monkeys reported by Girard et al.[41,42] from inflation tests. For the lamina modulus we considered ranges based on the literature,[5,39] based on ratios of lamina-to-sclera modulus or based on connective tissue volume density.[12,35] The main differences between the ranges were that those based on the literature allowed for slightly lower limits for scleral and lamina moduli (down to 1 and 0.1 MPa, respectively), and those based on inflation tests allowed for a higher limit for the scleral modulus (up to 34.5 MPa). After analysis, the material properties turned out to be among the most influential factors. Hence, we decided to evaluate the sensitivity of the results on the assumed material properties. For this we replicated the study, repeating all runs and analyses, using different material property ranges. Although varying the ranges affected slightly the relative influence of the factors, the main results remained consistent. Therefore, for clarity, we show results obtained with laminar properties based on the studies by Roberts et al.,[12,35] and scleral properties as an average of the values from the uniaxial[40] and inflation[41,42] tests, which were less than 10% different. Note that we use the term stiffness to represent the tissue mechanical properties, independent of geometry, and therefore cases with high or low Young's moduli are referred to as stiff or compliant, respectively. The concept of structural, or effective, stiffness is also useful and increasingly common,[13,21,42] since it combines the tissue mechanical properties with aspects of its geometry, such as thickness and shape.

Finite Element Discretization (Meshing)

For discretization and mesh improvement we followed the same methods as reported in several studies[29,30,43]: After the triangulated surfaces were morphed, the model volumes were meshed with four-node tetrahedra using target element sizes of 25, 50, and 125 μm for the lamina, peripapillary sclera, and scleral shell, respectively. The interior mesh was then iteratively smoothed and relaxed using Laplace's algorithm until the largest change in nodal locations was smaller than one fifth of a micrometer. For simulation and analysis the elements were converted to 10-noded tetrahedra by adding mid side nodes to the element edges. The nodal density necessary for accurate solution may depend on the parameter combinations and vary between models. Hence, the mesh refinement study had two parts. First, before morphing, we tested for sufficient nodal density in a baseline configuration. This nodal density was increased eight-fold (half target element-side length) and used as input for meshing the rest of the models. Second, after the simulations had been performed, we selected some cases with particularly large strains or deformations and tested whether these had been sufficiently refined. In every case, they were. The final models were formed by between 100,000 and 230,000 elements, depending on the geometry.

Boundary Conditions

The effects of IOP were modeled as a distributed load of 5 mm Hg acting on the element faces exposed to the interior of the eye. The magnitude of these forces was chosen to represent a modest increase in IOP from the eye fixation pressure (10 mm Hg) to an elevated level

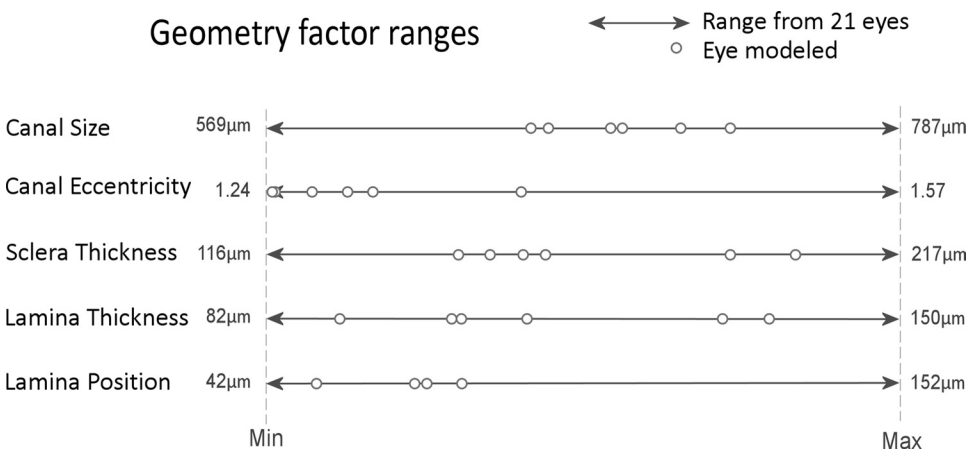

FIGURE 2. Geometry factor ranges. Geometry factor ranges were derived from histomorphometry of the ONH of 21 normal monkey eyes, 6 of which were used as models in this study (see the Methods section for details of the manuscripts in which these data have been presented). The range for each factor was defined as the minimum and maximum value of the measure over the 21 eyes. See Figure 1 for the factor definitions and Figure 3 for an illustration of models with various levels of the factors.

still within the normal range (15 mm Hg). The rationales for this choice are addressed in the Discussion section. The nodes on the equator were restricted to deform radially on the plane of the equator. Boundary conditions were defined on the baseline models and preserved through the morphing.

Outcome Measures

Two measures of IOP-induced deformation were computed for each model (Fig. 1): SCE, defined as the change in canal size (i.e., a change in mean anterior lamina insertion distance to its centroid), and LCD, defined as the change in LC position (i.e., change in mean anterior–posterior position of the anterior lamina surface relative to a least-squares plane fit to the anterior laminar insertion points). Both measures of change were computed like their parameter counterparts (canal size and lamina position), except for the need fit a new plane to the deformed anterior laminar insertion to compute the measures at increased IOP.

Experiment Design and Analysis

A two-level, full-factorial experimental design was selected for the seven continuous factors (Fig. 3).[31,32] The design was repeated six times to add the eye as a categorical (nominal) factor. Five extra runs were added to each combination of material properties, per eye, to evaluate pure error (such as drift).[31] Pure error was 0 for both re-

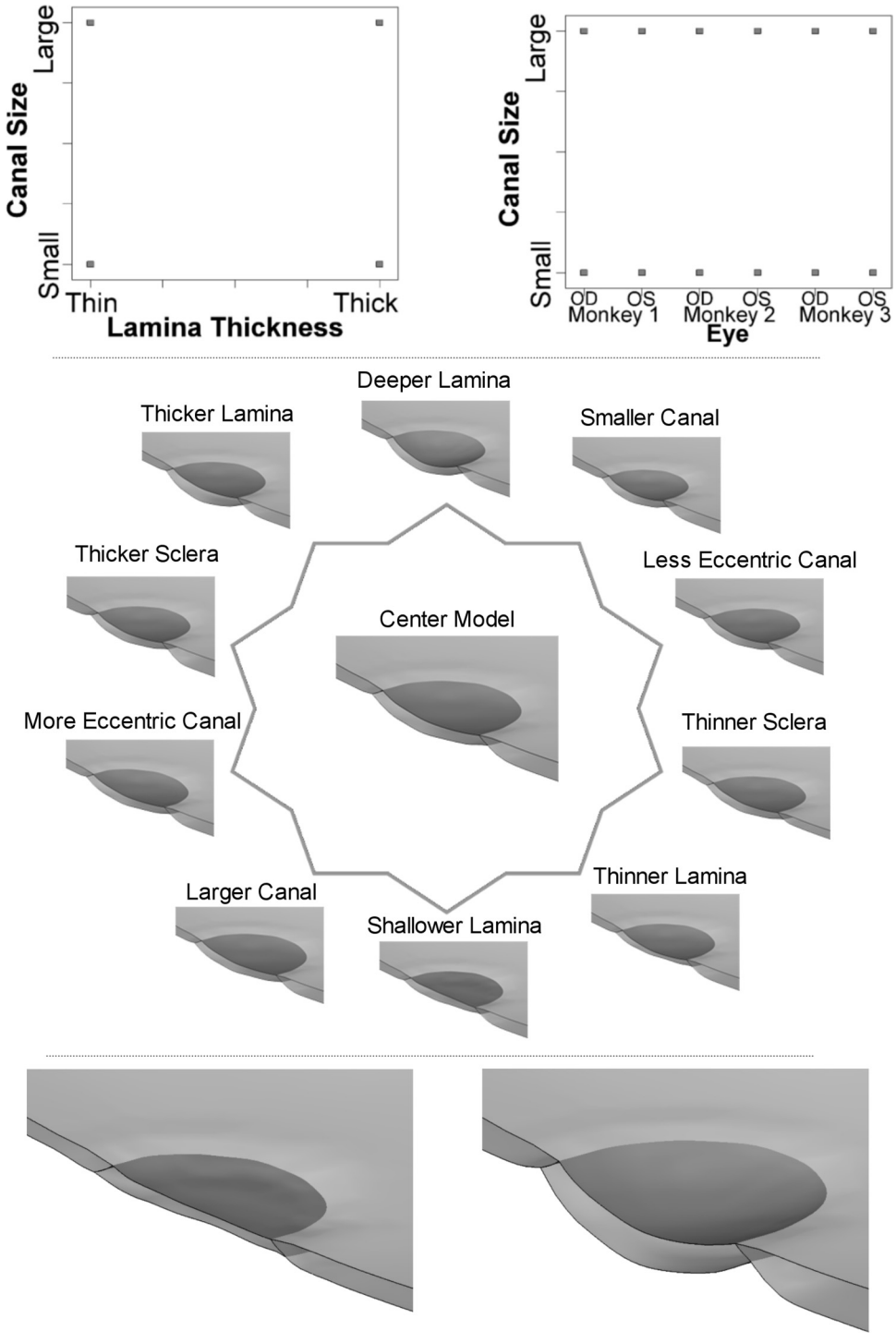

Figure 3. The experimental design and examples of model geometries and variations. Distribution of the factor combinations studied (*top row*). Shown are two-dimensional projections of the eight-dimensional parameter space. Note that in the two-level, full-factorial design all the models studied were at the corners of the factor space. Starting from a center model, five geometry factors were varied. Cutaway views of models produced by varying the factors one by one (*middle row*). Two extreme cases produced by setting all the factors at the low (*left side*, *bottom row*) or high (*right side*, *bottom row*) levels.

sponses. This method resulted in an orthogonal, balanced design with 888 model combinations [$(2^7 + 5 \times 4) \times 6 = 888$]. The order in which the models were prepared, run, and analyzed was randomized.

We used ANOVA to assess the significance ($P < 0.01$) and strength of factor and factor-interaction effects.[31,32] Specifically, we determined the relative influence of the factors and their interactions by comparing their percentage contribution to the total sum of squares corrected by the mean. The sum of squares is computed as the sum of the squared differences between an observation and the mean of all observations. It is common in factorial analysis to use the sum of squares over factor levels to represent the factor contributions. (For more details of this method and the supporting rationale, please see Refs. 21, 30–32.) The response variables were transformed to improve the normality of the responses and residuals, satisfy the requirements of ANOVA, and allow factor effects to be added in an unbiased fashion.[32] For LCD, it was necessary to add a constant (14.1765 μm) to make the values positive and sufficiently large to avoid numerical problems.[31] The responses were converted back to the original scale for plotting. A discussion of the rationale and consequences of the choice of 0.01 as the threshold for statistical significance has been published elsewhere.[21]

Results

IOP-induced LCD was between 53.6 μm (posteriorly) and −12.9 μm (anteriorly), whereas SCE was between 0.5 and 15.2 μm, all expansions (Table 2). LCD depended most strongly on laminar modulus, position, and thickness, whereas SCE depended most strongly on scleral modulus and thickness (Table 2, Fig. 4). There were several significant and strong interactions, with larger contributions to variance on LCD than on SCE (Table 2, Fig. 4). Both LCD and SCE were essentially insensitive to variations in scleral canal eccentricity or to the eye used as baseline. Some three-factor interactions were also statistically significant ($P < 0.01$), although their effects were relatively small.

Similar levels of LCD and SCE could be produced for various combinations of scleral modulus and thickness (Fig. 5, top row). In other words, from the perspective of LCD and SCE, scleral modulus and thickness could balance each other out. Likewise, similar levels of LCD and SCE could be obtained with various combinations of laminar modulus and thickness (Fig. 5, bottom row), although the surface was slightly tilted toward a larger influence of laminar modulus than thickness. As would be expected from what was described above, LCD was most sensitive to variations in laminar properties and SCE to variations in scleral properties. Interestingly, increased scleral structural stiffness (i.e., increased modulus or thickness) had different effects on LCD and SCE. The structurally stiffest sclera (stiff and thick) led to minimum SCE and maximum posterior LCD. Conversely, the structurally most compliant sclera (compliant and thin) led to maximum SCE and maximum anterior LCD.

To illustrate how the mechanical properties of the sclera and LC may combine to produce either anterior or posterior LCD and varying degrees of SCE, we prepared the four models shown in Figure 6. To simplify comparison, we chose models with the same geometry and varied the material properties of both tissues to the extremes of their ranges. More compliant sclera led to larger total posterior displacement of the ONH, reducing the posterior LCD (for a compliant lamina, red line) or increasing the anterior LCD (for a stiff lamina, blue line). These results have traditionally been explained as a compliant sclera pulling the lamina taut, leading to net lamina anterior LCD.

It may seem from the contributions to the sum of squares that the strength of the interactions was small, yet even a relatively small interaction can have a notable effect on the responses to IOP. From the interactions in Table 2 and Figure 4, we have selected some that we believe are of interest to the reader and illustrate the key sensitivities of LCD (Fig. 7) and SCE (Fig. 8). For example, deeper laminas generally displaced anteriorly, whereas shallow laminas were split, many displacing posteriorly and some anteriorly (those with a small canal and a stiff lamina). Stiffening the lamina had a much greater effect on predicted laminar displacement for shallow laminas, an effect that was magnified when the scleral canal was large. Deeper laminas always displaced anteriorly and were much less sensitive to changes in laminar stiffness or canal size.

Compared with the geometric parameters and scleral modulus, the lamina modulus is not as well characterized. The results shown above and previous studies,[5,12,22,26,36,39,44] suggest that the LC modulus plays an important role on the LCD. The interaction plots in Figure 9 illustrate the effects on LCD of the lamina modulus and of its interactions with other parameters. It is clear that there are strong factor interactions, including lamina modulus with canal size, lamina thickness, and position.

Table 2. Fraction of the Sum of Squares Corrected by the Mean Contributed by the Factors, Independently or in Interaction

Factor	LCD	SCE
Independent		
Scleral canal size	3.8	3.2
Scleral canal eccentricity	0.0‡	0.0*
Sclera thickness	4.4	36.1
Lamina cribrosa thickness	7.2	0.0*
Lamina cribrosa position	21.3	2.3
Sclera modulus	3.9	45.8
Lamina cribrosa modulus	24.4	3.8
Eye	0.5	2.0
Interactions		
Canal size–lamina position	4.0	0.0*
Canal size–lamina modulus	5.7	0.1
Sclera thickness–sclera modulus	1.7	2.6
Sclera modulus–lamina modulus	0.1	1.1
Lamina thickness–lamina position	4.2	0.0*
Lamina thickness–lamina modulus	3.8	0.0*
Lamina position–sclera modulus	1.2	0.6
Lamina position–lamina modulus	4.9	0.6
Canal size–lamina position–lamina modulus	0.8	0.0*
Sclera modulus–lamina position–lamina modulus	0.1	0.2
All interactions combined	34.6	6.8
Distribution of actual values		
Maximum, μm	53.6	15.2
Mean, μm	3.4	4.2
Minimum, μm	−12.9	0.5
SD, μm	10.9	3.4
Model total sum of squares	935.7	453.0

Larger numbers represent a stronger influence of the factor or interaction on the response. For analysis, the responses were transformed by square root. All contributions, except those marked ‡, were statistically significant ($P < 0.01$). All statistically significant interactions were considered for the line labeled "All interactions combined", although, for clarity, only those with the strongest effects are shown explicitly. Note that for LCD positive values correspond to a posterior displacement. LCD was influenced most strongly by lamina cribrosa modulus and position, whereas SCE by scleral modulus and thickness. See Figure 4 for a graphic representation.

* Not statistically significant.

Discussion

The main goal of this work was to study LCD (anterior–posterior LC displacement) and SCE (scleral canal expansion) in response to acute increases in IOP. Specifically our objective

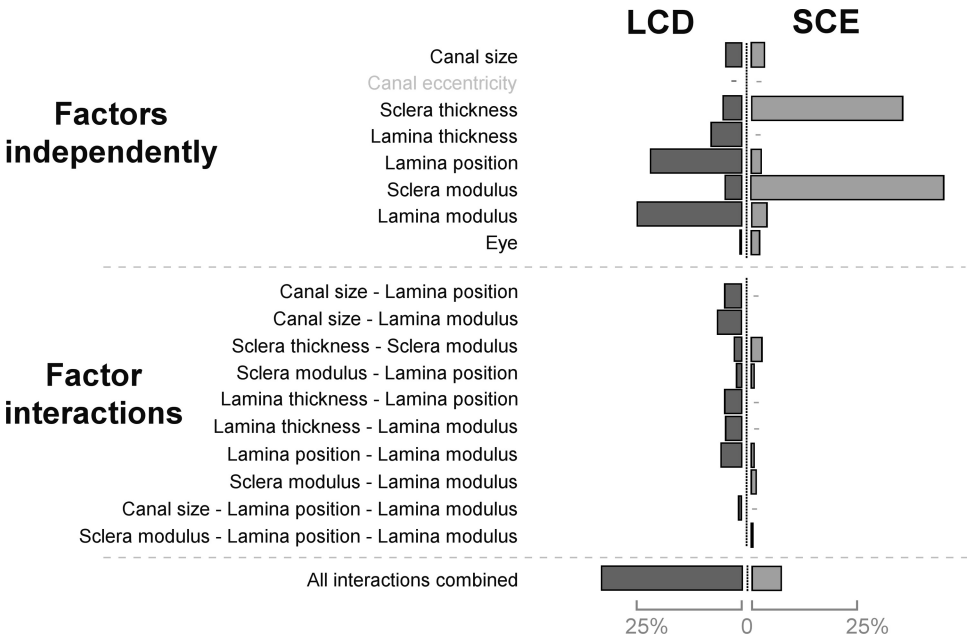

FIGURE 4. Graphical representation of the relative magnitude of the factor and interaction influences shown in Table 2. The bar lengths are proportional to the magnitude of the numbers in the table and are intended to simplify seeing the influences at-a-glance. Factors with a statistically significant effect ($P < 0.01$) are shown with a *bar*, the rest with a *gray dash*. Canal eccentricity is included here for completeness. The influential factors were different for each response: LCD was most influenced by lamina position and modulus, whereas SCE was most influenced by scleral thickness and modulus. Both responses were influenced by interactions, LCD more strongly than SCE. Recall that interactions may be interpreted as curvature in response space. Hence, relatively small contributions to the sum of squares in Table 2 (short bars in the figure) may still have large effects on the response within some regions of the factor space.

was to determine how these responses depend on seven factors: scleral canal size (radius) and eccentricity; scleral thickness and modulus (stiffness); and LC thickness, position and modulus (stiffness). For this we used parameterized, eye-specific models of normal monkey eyes. Two main conclusions arise: First, LCD and SCE depended on different factors, with LCD most strongly dependent on laminar position and modulus and SCE on scleral thickness and modulus. Second, there were several influential factor interactions, with stronger effects on LCD than on SCE.

LCD and SCE Depended on Different Factors

The large influences of the scleral modulus and thickness on SCE are consistent with previous studies wherein the properties of the sclera have been noted to be among the most influential on IOP-related ONH biomechanics.[5,21,22,26,39] The strong dependence of LCD on various properties of the lamina itself, even when considering simultaneous scleral deformations, had been speculated on,[1,3,12,25] but not demonstrated quantitatively. Although LCD and SCE were each most strongly

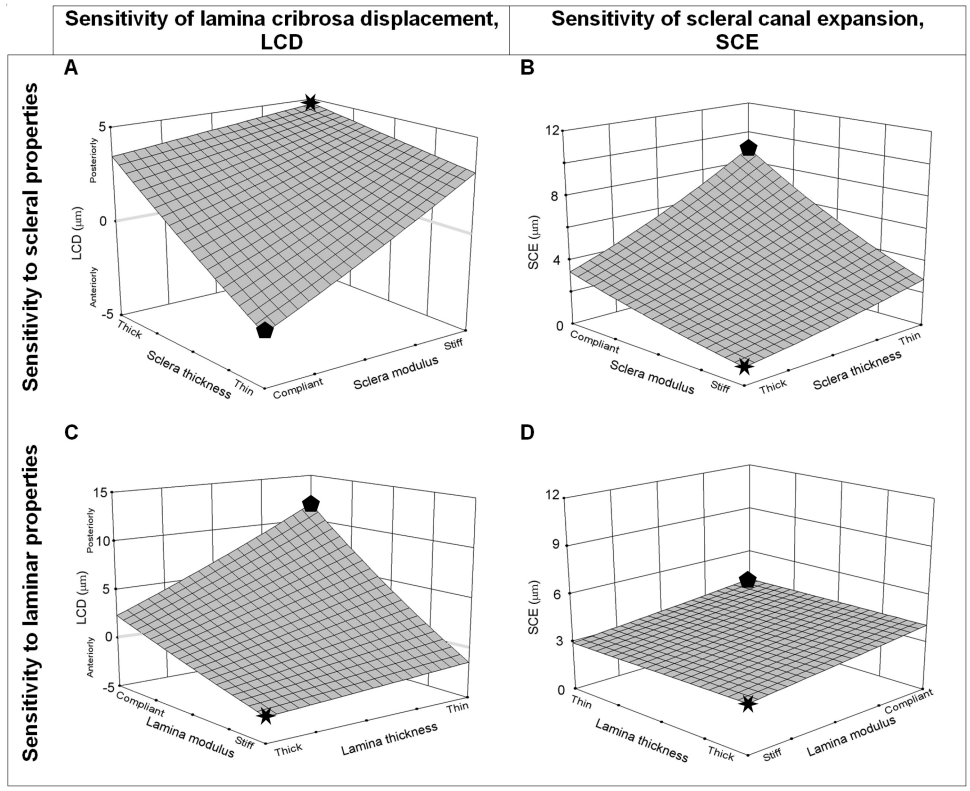

FIGURE 5. Sensitivity of LCD and SCE to laminar and scleral thickness and modulus. Effects of scleral and laminar thickness and modulus on LCD (**A**, **C**) and SCE (**B**, **D**). Similar levels of LCD and SCE could be produced for various combinations of scleral modulus and thickness. A similar effect could be obtained from the laminar modulus and thickness, although they do not balance as symmetrically. *Star*: combinations with the maximum effective stiffness (thick and stiff tissue); *pentagon*: combinations with the minimum effective stiffness (thin and compliant tissue). Note the different ranges in the *y*-axes (LCD) between (**A**) and (**C**). The axes' ranges were chosen to illustrate clearly the factor interaction. The smaller range in (**A**) than in (**B**) illustrates the limited influence on LCD of the scleral properties compared with the laminar properties.

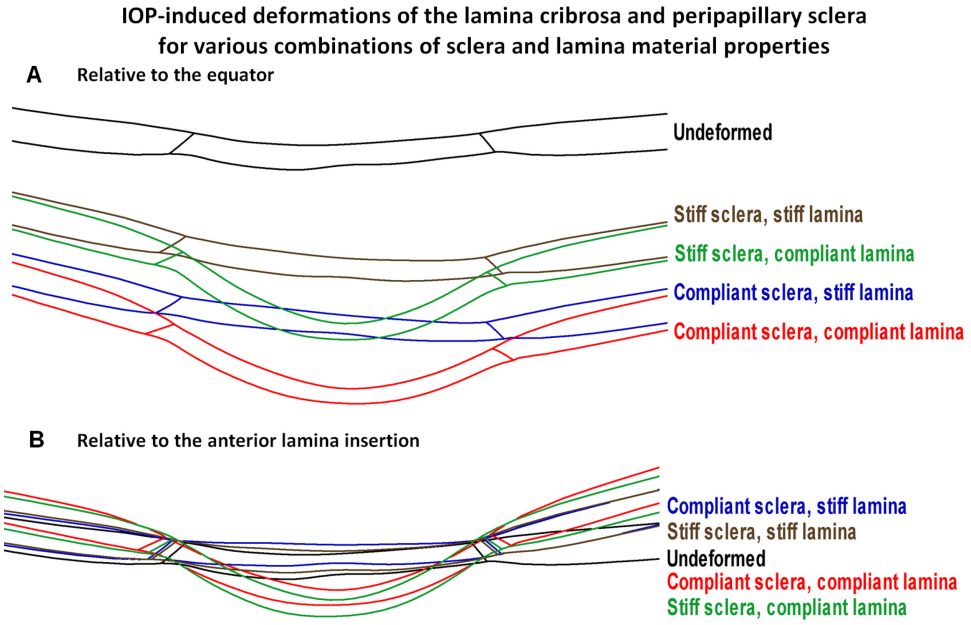

Figure 6. Examples of models with various combinations of scleral and laminar material properties. Cross sections through a model with the geometry of monkey 1 at the center of the parameter space in the undeformed (*black line*, 10 mm Hg IOP) and in the deformed state (*colored lines*, 15 mm Hg IOP). The deformations are relative to the equator to illustrate global deformations (*top*), or relative to the anterior laminar insertion to highlight local deformations (*bottom*), and have been exaggerated 10-fold. In the *top* panel it is easy to distinguish the cases with the compliant sclera (*blue* and *red*) by the large posterior displacement of the whole ONH. Similarly, in the *bottom* panel it is easy to distinguish the cases with the compliant lamina (*green* and *red*) by the large posterior displacement of the lamina. Note the anterior laminar displacement (negative LCD), larger for compliant sclera and stiff lamina (*blue*) than for both tissues stiff (*brown*). A stiff lamina also reduced the bending, or bowing, of the peripapillary sclera.

sensitive to two factors, one material and one geometric, they were also highly sensitive to other factors. This was especially clear for LCD, which was also sensitive to LC thickness, canal size, and scleral thickness and modulus.

There Were Influential Factor Interactions for Both LCD and SCE

The contribution of the factor interactions to the sum of squares—approximately 7% on SCE and 35% on LCD (Table 2, Fig. 4)—may be interpreted as if LCD and SCE are relatively insensitive to factor interactions. However, as we have illustrated with the interaction plots (Figs. 7, 8, 9), factor interactions still have a critical role in the responses. This is because the factor interaction strengths according to the sum of squares are global influences (i.e., averages over the whole factor space). An interaction means that the strength of the influence of a factor on a response depends on another factor and therefore varies from one region of the factor space to another and may not be well represented by the average. When interactions are present or factor effects are nonlinear, as is the case in this work, from a global measure of influence one cannot tell if a factor influence is strong in a small region of the factor space or weak over a large region. Compounding this difficulty is the fact that factor influences are relative measures, and therefore an increased influence for one factor reduces the relative influence of another. These phenomena have been described for ONH biomechanics in one previous work.[21] Hence, in general, ranking of factors by influence can be misleading and must be interpreted accordingly. Despite this, we chose to include Table 2 and Figure 4, because we believe that they illustrate clearly how certain factors were substantially more influential than others.

LCD was influenced by several interactions, altogether contributing about a third of the response variance. This finding shows that factors affecting LCD combine in complex ways, that LCD is strongly dependent on the specific combination of factors (i.e., the particular properties of an eye), and therefore that it is difficult to predict IOP-induced LCD from a few factors. This helps explain the large variability in the experimental measurements of IOP-induced LCD (Burgoyne CF, et al. *IOVS* 2008;49:ARVO E-Abstract 3655; Agoumi Y, et al. *IOVS* 2009;50:ARVO E-Abstract 4898).[8–11,24,25,28,33,34,38,45] It also suggests that it is important to continue development of experimental techniques to measure all the factors involved and not just laminar position and modulus.

SCE was less sensitive to interactions than LCD, with interactions between scleral thickness and scleral modulus and between scleral and lamina moduli being the strongest. The first interaction can be interpreted as the structural stiffness of the scleral shell (i.e., a combination of scleral material properties and geometry), as discussed elsewhere.[3,13,21,23,41,46,47] The second interaction can be interpreted as the role of laminar stiffness in the expansion of the scleral canal: increased lamina modulus (stiffer) reducing canal expansion, more so when the sclera was compliant than when it was stiff (Fig. 6). We have noted and discussed the sensitivity of canal expansion to laminar stiffness.[12,13]

In describing the effects of IOP on the LC, a useful conceptual framework has emerged in the past few years: that of the balance between the direct effects of IOP "pushing" the lamina posteriorly and the indirect effects of IOP deforming the sclera, expanding the canal, which in turn "pulls" the lamina taut from the sides.[3,12,23,25,47,48] Within this framework, a stiff sclera would deform little, with a small canal expansion (i.e., not

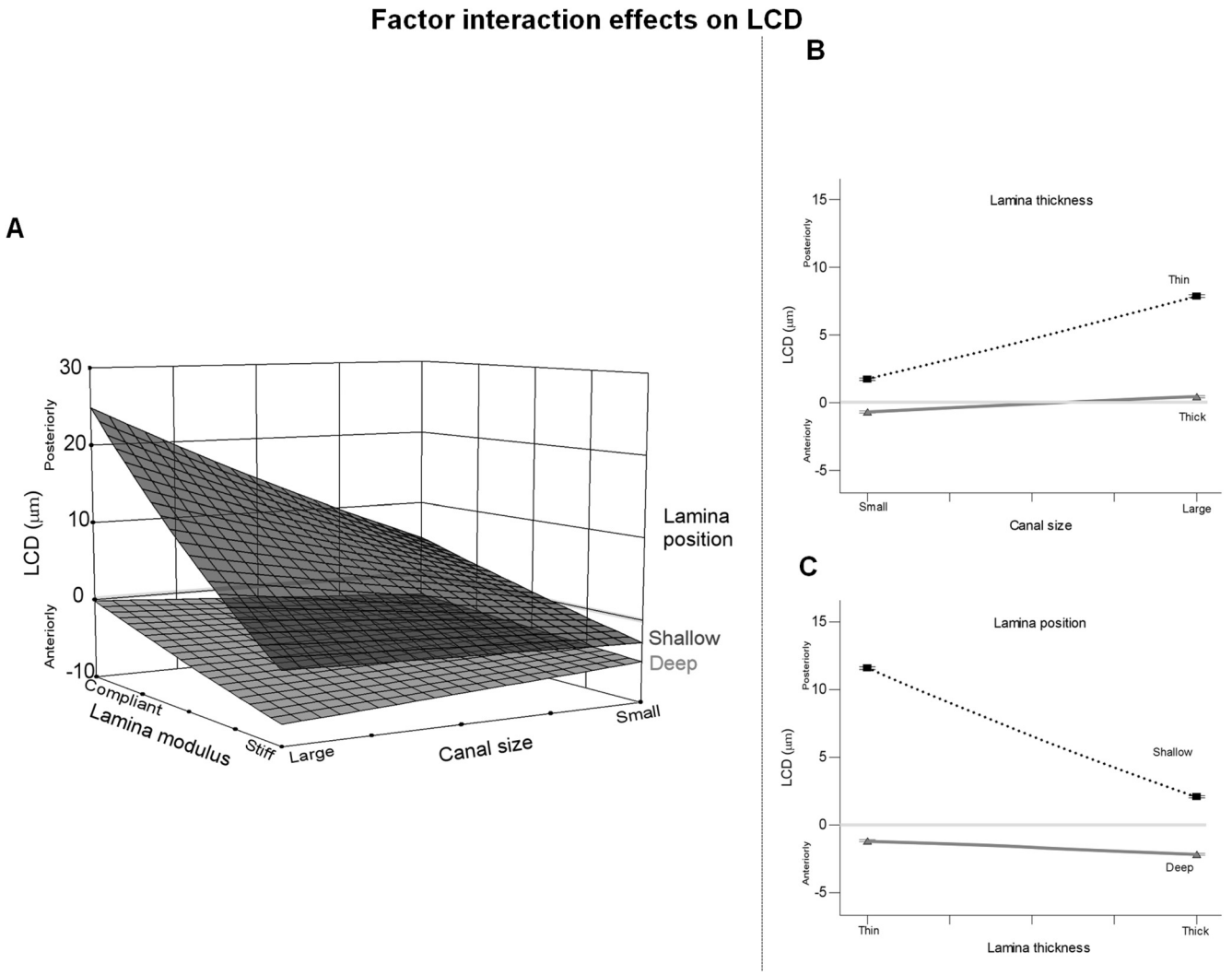

FIGURE 7. Sensitivity of LCD to laminar modulus, position and thickness and to canal size. (**A**) The three-factor interaction involving the laminar modulus, lamina position, and canal size. The effect of laminar position is represented by the distance between the surfaces. Deeper laminas tended to displace anteriorly, whereas the shallow laminas could displace anteriorly or posteriorly depending on the size of the canal and the laminar modulus. When the lamina was deep (bottom surface) the effects of the two other factors were smaller than when the lamina was shallow (upper surface)—that is, the top surface is steeper than the bottom surface. The effects of stiffening of the LC were larger when the canal was large than when it was small, and when the lamina was shallow than when it was deep. (**B**, **C**) Two traditional interaction plots. In the interaction between lamina thickness and canal size the effects of canal size were larger when the lamina was thin than when it was thick. Conversely, lamina thickness had a larger influence when the canal was large than when it was small. For the interaction between lamina thickness and position, lamina thickness reduced LCD when the lamina was shallow, but not when the lamina was deep. Conversely, when the lamina was thick its position had little influence on LCD, but when the lamina was thin the position had large influence. Thicker, stiffer or deeper laminas within a small canal had smaller posterior displacements and were more likely to displace anteriorly. Factors not explicitly varied were at the center levels.

pulling the lamina taut), resulting in the LC displacing posteriorly. Conversely, a compliant sclera would deform more, pull the lamina taut from the sides, and result in a shift of LCD anteriorly (less posteriorly or more anteriorly). The results of this work, exemplified by Figure 6, support the conceptual framework. However, we have also shown that the sensitivity of LCD to scleral and laminar properties is complex, and therefore the extent to which the conceptual framework generalizes is still to be determined. Note that even for small LCDs or SCEs, the strains and stresses within the laminar and scleral tissues could be substantial.[6] This possibility should be considered when interpreting measurements of acute deformation and their implications on sensitivity to IOP.

The two responses analyzed in this work were chosen because we believe they represent important aspects of the response of the ONH to changes in IOP. We are not the first to study them. Measurements of IOP-related LCD and SCE have been made using radiographic[10,11] and 2D[8,9,45,49,50] or 3D histomorphometric techniques,[24,25,27,28,33,34,38] and with optical coherence tomography imaging (Agoumi Y, et al. *IOVS* 2009;50:ARVO E-Abstract 4898). Although valuable, the variability in the ONH's response to changes in IOP, the difficulties of accessing the interior of the ONH (as opposed to imaging the surface of the disc), and the lack of a full characterization of the geometry and material properties of each eye have prevented the experimental approaches from providing a detailed picture of LCD and SCE and of their sensitivity to the geometry and material properties of the tissues. The ability to measure LC position reliably is in development (Burgoyne CF, et al. *IOVS* 2008;49:ARVO E-Abstract 3655; Agoumi Y, et al. *IOVS* 2009;50:ARVO E-Abstract 4898),[51–54] and none of the studies cited above reported the factors identified in this work

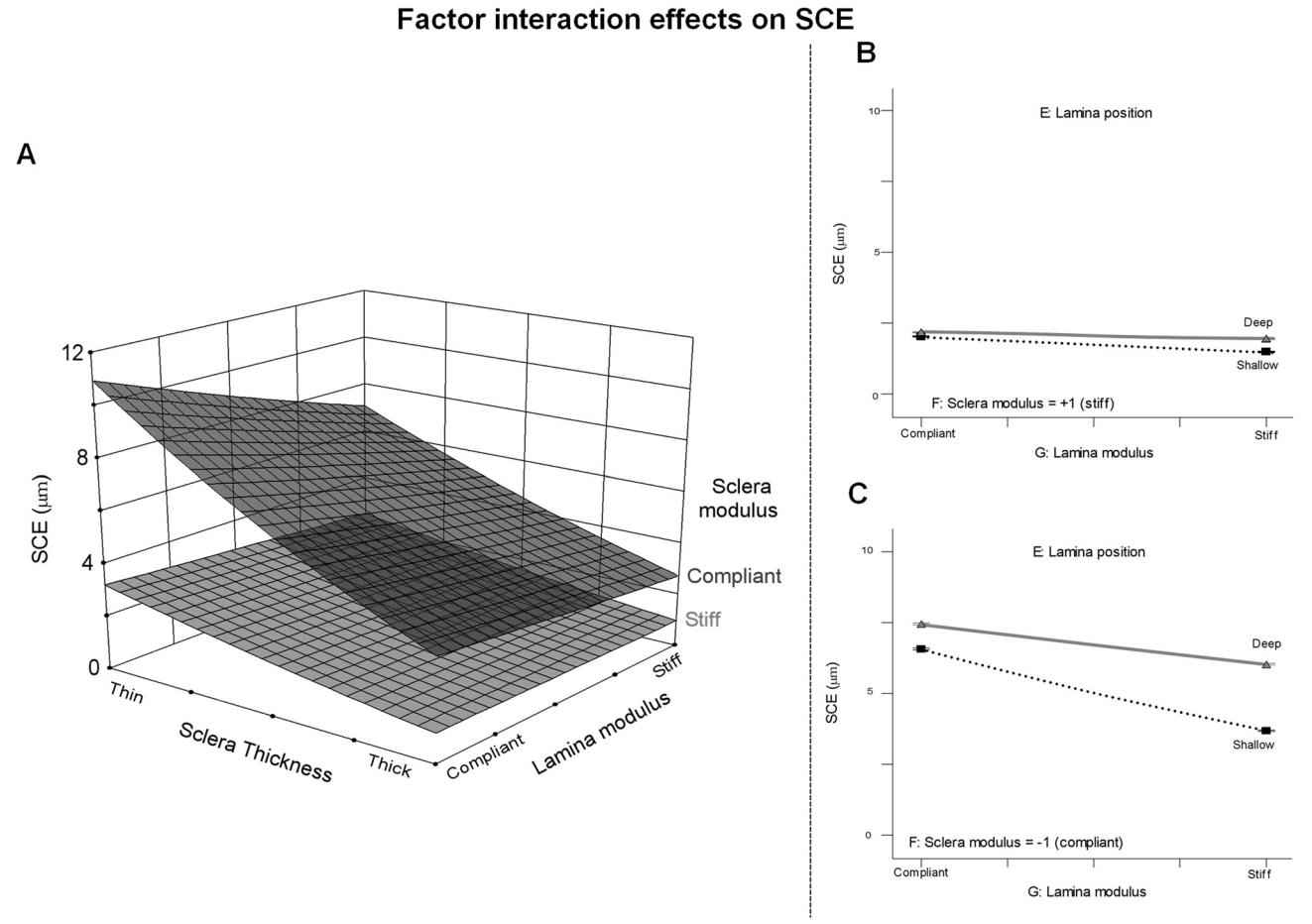

FIGURE 8. Sensitivity of SCE to scleral modulus and thickness and laminar modulus and position. (**A**) The distance between the surfaces is the effect of the sclera modulus. When the sclera was stiff (bottom surface) the effects of the other two factors were smaller than when the sclera was compliant (top surface). Similarly, when the sclera was thick (right side), stiffening the lamina or the sclera had smaller effects than when the sclera was thin (left side). (**B**, **C**) The effects of laminar position and modulus, and how their effects depend also on the sclera modulus. When the sclera was stiff (**B**), neither lamina modulus nor lamina position affected an already low SCE. However, when the sclera was compliant (**C**), SCE was reduced by increased lamina modulus, more so if the lamina was shallow than if it was deep. Conversely, the laminar position reduced SCE slightly if the lamina was compliant and substantially if it was stiff. (**B**, **C**). These plots illustrate how the lamina could influence SCE, if the circumstances were right (e.g., when the sclera was compliant and thin and the lamina shallow).

measured as the most influential on LCD and SCE. This may explain why previous studies were unable to identify good predictors for IOP-related LCD and SCE. To the best of our knowledge, this study is the first to consider factor interactions on LCD and SCE. We are working on extending the responses analyzed to include other measures of the effects of IOP, either because they are potentially biologically important, such as the stresses and strains,[6,55,56] or because they could be measured in an experiment, such as altered blow flow.[57]

Compared with other numerical studies, we believe the approach adopted in this work has several advantages. First, this study is based on eye-specific models, which incorporate more of the characteristics that represent a realistic ONH than do generic models. Second, the parameterization techniques[29,30,43] (the morphing) allowed us to evaluate the effects of interactions between geometry and material properties and to demonstrate that they are important. Our previous study on the effects of factor interactions in ONH biomechanics focused on IOP-related stress and strain[21] and did not evaluate LCD and SCE. These responses are potentially clinically measurable. Another strength of this study is that we used updated information on the ranges of tissue geometry and material properties. As we have discussed elsewhere,[5,21,39] unnaturally large ranges can make factors artificially influential and attenuate the influence of other factors. Previous sensitivity studies used factor information from the literature, often spanning several species, treatments, and testing procedures.[5,12,21,39,44] Herein, we used factor ranges derived from our own measurement of the normal monkey ONH, compiled in a way that optimized their applicability to this study (e.g., all factors were measured in the same samples).

We acknowledge some degree of arbitrariness in the choice of factors, particularly of the material properties. The ranges of the geometric factors are conservative, since they are the ranges observed in a relatively small sample of 21 eyes. We consider our method for defining the ranges for material properties reasonable given the information available and the assumptions on material properties (see the following text for a discussion of this point). Still, since the material properties turned out to be among the most influential factors we evaluated the sensitivity of the results and conclusions to the assumed material ranges. Although varying the ranges affected slightly the relative influences of the factors, the main results remained consistent, which suggests that the results and conclusions are robust. We will continue to work to improve the characterizations of lami-

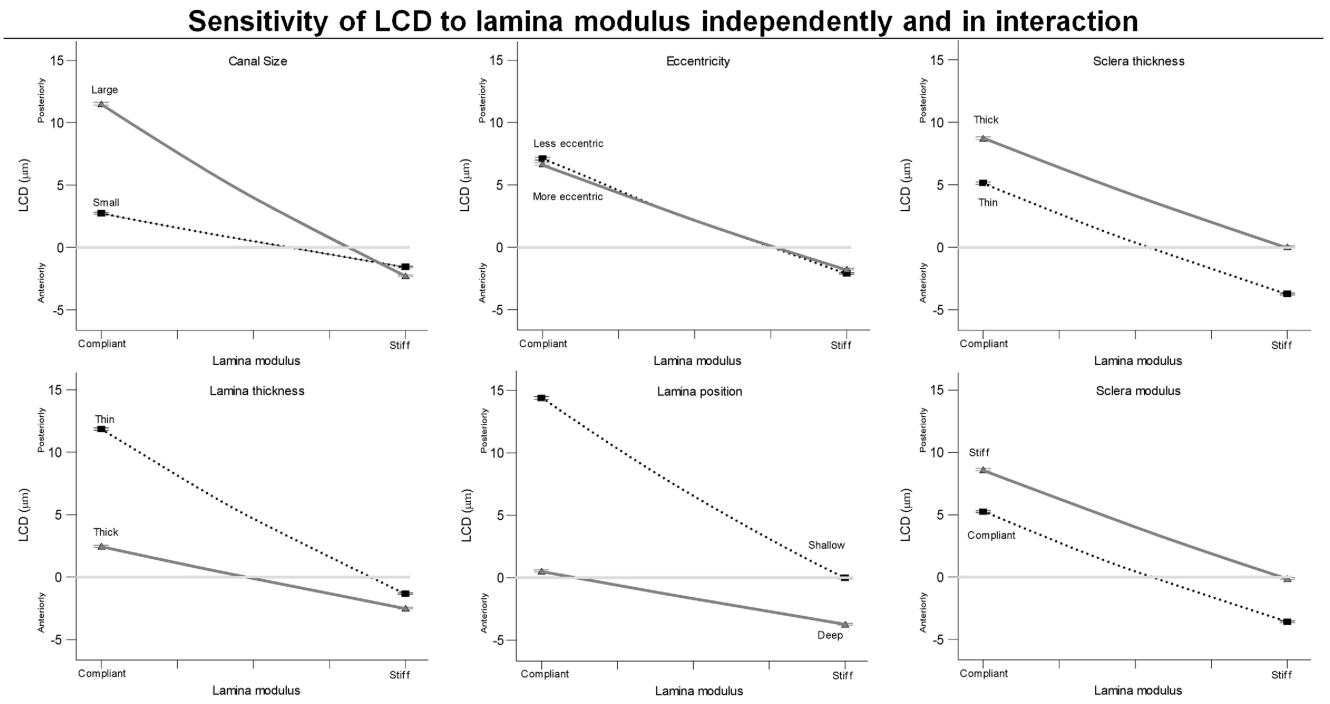

FIGURE 9. Sensitivity of LCD to the laminar modulus, independently and in interaction with six other factors. Each plot illustrates the effects of an interaction between the lamina and a second factor. The line slope indicates the sensitivity to laminar modulus, whereas the distance between the lines indicates the influence of the second factor. For example, eccentricity had almost no effect, and so both lines overlap. Increased lamina modulus always resulted in more anterior displacement (or reduced posterior displacement). Nonparallel lines indicate an interaction since the effect of one factor depends on the level of the other factor. LCD was more sensitive to laminar modulus when the canal was large, when the lamina was thin or when it was shallow. The stiffness and modulus of the sclera affected LCD but did not interact with the laminar modulus (i.e., the lines in the two rightmost plots are parallel).

nar and scleral properties and to determine how they influence ONH biomechanics.

This study also differs from previous work on LCD and SCE in our use of a relatively small (5 mm Hg) acute increase in IOP. We did this for several reasons: First, normal IOP is much more common than elevated IOP, and therefore small variations in IOP are relevant to a larger group. Second, small IOP elevations may be particularly informative in understanding the pathogenesis of low-tension glaucoma. Third, as we have demonstrated here, ONH biomechanics are complex, even with simplified geometries and material properties. Simulating a relatively small IOP increase allowed us to use linear materials, the stiffness of which can be specified by a single parameter for each tissue—the Young's modulus. Finally, we believe that providing a solid understanding of ONH biomechanics at low pressures helps build an understanding of larger pressure increases. It is important to point out that the effects of IOP do not necessarily scale linearly with the increase in IOP, even in models with linear materials.

This work should be interpreted in light of assumptions, explicit or implicit, in the models. We have previously discussed issues related to the construction of the baseline models[12,13,35] and to the choice of material properties.[5,26,39] Simulating larger increases in IOP will probably necessitate the use of nonlinear material properties. We are working on models with more realistic material properties (inhomogeneous, anisotropic, and nonlinear sclera[7,41,42,58,59] and inhomogeneous and anisotropic lamina[7,12,13,35,36,60]) and various loading conditions (IOP insult and cerebrospinal fluid pressure[17,61–64]). In light of these assumptions, the absolute magnitudes of the predictions should be interpreted carefully. We believe, however, that the relative magnitudes, which encode the factor influences, are robust. The models represent an acute deformation of the tissues due to increases in IOP and do not account for viscoelastic effects or tissue remodeling. The consequences of introducing these complexities are difficult to predict, because their effects are nonlinear and because they are further complicated by the interactions between tissue properties and other factors.[21]

Despite being based on eye-specific geometries, the models are still simplified. They do not completely reflect the complex architecture of the ONH region, and the scleral shell variations in thickness were not eye-specific. The models do not include pre- or postlaminar neural tissue or the pia mater, as other models did[6,27,65] and therefore cannot be used to predict the mechanics of these tissues, which may be useful in relating the model predictions with experiments and may be relevant for understanding the physiologic consequences of IOP. It is also possible that we did not morph all the key factors that determine LCD and SCE. The morphing, by design, was dependent on the six eye-specific geometries and therefore may not represent all the variations and details possible. All six eyes had similar sensitivities to the factors, and the factor "eye" (the baseline eye-specific geometry) was therefore among the least influential factors. This outcome gives us confidence that the geometries and variations considered span reasonable physiologic ranges and represent the key factors. It also suggests that, for studies focusing on factor influences over the whole factor space, it may not be necessary to analyze several eyes. Still, given the factor interactions, we expect local sensitivity to vary between individuals. The models and analysis were based on the normal monkey eye, which is smaller and has a thinner LC and sclera than the human eye.[46,66,67] The baseline geometries and the ranges over which the geomet-

ric factors were varied were derived from 3D reconstructions and histomorphometry that may have been affected by artifacts from the embedding and fixation, such as tissue shrinkage. These artifacts and how they may affect the results from histomorphometry are discussed in detail elsewhere.[24,25,28,33,34,38] All the geometric factors, however, were derived from the same reconstructions, and hence the factors are mutually consistent. Large variations in tissue geometry and material properties also occur normally or in pathologic conditions, such as the enlarged disc, thinned LC and sclera, and altered scleral mechanical properties associated with myopia.[68,69] These alterations have been hypothesized to be important contributors to susceptibility to IOP,[1,5,68,69] and in future work we will extend the parameter ranges to study them.

Notwithstanding the differences between monkey and human eyes, we anticipate that the main conclusions derived in this work apply to human eyes as well. Specifically, we predict that in human eyes LCD and SCE depend on different factors and that there are several influential interactions between factors. However, the specific factors influencing each response and the strength of their interactions may or may not be the same in the human and monkey. The difficulty in predicting ONH biomechanics increases rapidly with the number of influential factors and the magnitude of IOP elevation.

In summary, we used numerical techniques to study the anterior–posterior LC deformation and the scleral canal expansion associated with acute changes in IOP. LC deformation was most sensitive to laminar position and modulus, whereas scleral canal expansion was most sensitive to scleral thickness and modulus. For both responses, there were strong interactions between factors, suggesting that the effects of IOP on the ONH are the result of a complex combination of several factors. This work is important because it lays the foundation for understanding the origins of the range of individual sensitivities to IOP and the individual risk for the development and progression of glaucomatous neuropathy. Moreover, the outcome measures—LCD and SCE—are likely to be accessible by in vivo measurement in the near future,[51–54] as will some of the geometric parameters used in our analysis. Combining such measurements with sensitivity analyses may allow inferences to be made regarding changes in tissue compliance over time in individual patients, a potentially powerful biomarker for assessing risk of glaucomatous neuropathy.

Acknowledgments

The authors thank Jonathan Grimm and Juan Reynaud for developing code and scripts.

References

1. Burgoyne CF, Downs JC, Bellezza AJ, Suh JK, Hart RT. The optic nerve head as a biomechanical structure: a new paradigm for understanding the role of IOP-related stress and strain in the pathophysiology of glaucomatous optic nerve head damage. *Prog Retin Eye Res.* 2005;24:39–73.
2. Quigley HA. Glaucoma: macrocosm to microcosm the Friedenwald lecture. *Invest Ophthalmol Vis Sci.* 2005;46:2662–2670.
3. Sigal IA, Ethier CR. Biomechanics of the optic nerve head. *Exp Eye Res.* 2009;88:799–807.
4. Kirwan RP, Crean JK, Fenerty CH, Clark AF, O'Brien CJ. Effect of cyclical mechanical stretch and exogenous transforming growth factor-beta1 on matrix metalloproteinase-2 activity in lamina cribrosa cells from the human optic nerve head. *J Glaucoma.* 2004; 13:327.
5. Sigal IA, Flanagan JG, Ethier CR. Factors influencing optic nerve head biomechanics. *Invest Ophthalmol Vis Sci.* 2005;46:4189–4199.
6. Sigal IA, Flanagan JG, Tertinegg I, Ethier CR. Predicted extension, compression and shearing of optic nerve head tissues. *Exp Eye Res.* 2007;85:312–322.
7. Grytz R, Meschke G. A computational remodeling approach to predict the physiological architecture of the collagen fibril network in corneo-scleral shells. *Biomech Model Mechanobiol.* 2010; 9:225–235.
8. Yan DB, Metheetrairut A, Coloma FM, Trope GE, Heathcote JG, Ethier CR. Deformation of the lamina cribrosa by elevated intraocular pressure. *Br J Ophthalmol.* 1994;78:643.
9. Yan DB, Coloma FM, Metheetrairut A, Trope GE, Heathcote JG, Ethier CR. Deformation of the lamina cribrosa by elevated intraocular pressure. *Br J Ophthalmol.* 1994;78:643–648.
10. Levy NS, Crapps EE. Displacement of optic nerve head in response to short-term intraocular pressure elevation in human eyes. *Arch Ophthalmol.* 1984;102:782–786.
11. Levy NS, Crapps EE, Bonney RC. Displacement of the optic nerve head. Response to acute intraocular pressure elevation in primate eyes. *Arch Ophthalmol.* 1981;99:2166–2174.
12. Roberts MD, Liang Y, Sigal IA, et al. Correlation between local stress and strain and lamina cribrosa connective tissue volume fraction in normal monkey eyes. *Invest Ophthalmol Vis Sci.* 2010; 51:295–307.
13. Roberts MD, Sigal IA, Liang Y, Burgoyne CF, Downs JC. Changes in the biomechanical response of the optic nerve head in early experimental glaucoma. *Invest Ophthalmol Vis Sci.* 2010;51: 5675–5684.
14. Zeimer RC, Ogura Y. The relation between glaucomatous damage and optic nerve head mechanical compliance. *Arch Ophthalmol.* 1989;107:1232–1234.
15. Wells AP, Garway-Heath DF, Poostchi A, Wong T, Chan KC, Sachdev N. Corneal hysteresis but not corneal thickness correlates with optic nerve surface compliance in glaucoma patients. *Invest Ophthalmol Vis Sci.* 2008;49:3262–3268.
16. Edwards ME, Good TA. Use of a mathematical model to estimate stress and strain during elevated pressure induced lamina cribrosa deformation. *Curr Eye Res.* 2001;23:215–225.
17. Morgan WH, Chauhan BC, Yu DY, Cringle SJ, Alder VA, House PH. Optic disc movement with variations in intraocular and cerebrospinal fluid pressure. *Invest Ophthalmol Vis Sci.* 2002;43:3236–3242.
18. Meredith SP, Swift L, Eke T, Broadway DC. The acute morphologic changes that occur at the optic nerve head induced by medical reduction of intraocular pressure. *J Glaucoma.* 2007;16:556–561.
19. Lesk MR, Spaeth GL, Azuara-Blanco A, et al. Reversal of optic disc cupping after glaucoma surgery analyzed with a scanning laser tomograph. *Ophthalmology.* 1999;106:1013–1018.
20. Albon J, Purslow PP, Karwatowski WS, Easty DL. Age related compliance of the lamina cribrosa in human eyes. *Br J Ophthalmol.* 2000;84:318–323.
21. Sigal IA. Interactions between geometry and mechanical properties on the optic nerve head. *Invest Ophthalmol Vis Sci.* 2009;50: 2785–2795.
22. Sigal IA, Flanagan JG, Tertinegg I, Ethier CR. Modeling individual-specific human optic nerve head biomechanics, I: IOP-induced deformations and influence of geometry. *Biomech Model Mechanobiol.* 2009;8:85–98.
23. Girard MJ, Downs JC, Burgoyne CF, Suh JK. Peripapillary and posterior scleral mechanics, I: development of an anisotropic hyperelastic constitutive model. *J Biomech Eng.* 2009;131:051011.
24. Yang H, Downs JC, Girkin C, et al. 3D histomorphometry of the normal and early glaucomatous monkey optic nerve head: lamina cribrosa and peripapillary scleral position and thickness. *Invest Ophthalmol Vis Sci.* 2007;48:4597–4607.
25. Yang H, Downs JC, Sigal IA, Roberts MD, Thompson H, Burgoyne CF. Deformation of the normal monkey optic nerve head connective tissue after acute IOP elevation within 3D histomorphometric reconstructions. *Invest Ophthalmol Vis Sci.* 2009;50:5785–5799.
26. Sigal IA, Flanagan JG, Tertinegg I, Ethier CR. Finite element modeling of optic nerve head biomechanics. *Invest Ophthalmol Vis Sci.* 2004;45:4378–4387.
27. Sigal IA, Flanagan JG, Tertinegg I, Ethier CR. 3D morphometry of the human optic nerve head. *Exp Eye Res.* 2010;90:70–80.

28. Yang H, Thompson H, Roberts MD, Sigal IA, Downs JC, Burgoyne CF. Deformation of the early glaucomatous monkey optic nerve head connective tissue following acute IOP elevation within 3D histomorphometric reconstructions. *Invest Ophthalmol Vis Sci*. Published online August 11, 2010. [Epub ahead of print.]
29. Sigal IA, Yang H, Roberts MD, Downs JC. Morphing methods to parameterize specimen-specific finite element model geometries. *J Biomech.* 2010;43:254–262.
30. Sigal IA, Whyne CM. Mesh morphing and response surface analysis: quantifying sensitivity of vertebral mechanical behavior. *Ann Biomed Eng.* 2010;38:41–56.
31. Anderson MJ, Whitcomb PJ. DOE Simplified: practical tools for effective experimentation. New York: Productivity Press; 2000; 256.
32. Montgomery DC. *Design and Analysis of Experiments.* New York: Wiley; 2004;660.
33. Downs JC, Yang H, Girkin C, et al. Three-dimensional histomorphometry of the normal and early glaucomatous monkey optic nerve head: neural canal and subarachnoid space architecture. *Invest Ophthalmol Vis Sci.* 2007;48:3195–3208.
34. Yang H, Downs JC, Burgoyne CF. Physiologic intereye differences in monkey optic nerve head architecture and their relation to changes in early experimental glaucoma. *Invest Ophthalmol Vis Sci.* 2009;50:224–234.
35. Roberts MD, Grau V, Grimm J, et al. Remodeling of the connective tissue microarchitecture of the lamina cribrosa in early experimental glaucoma. *Invest Ophthalmol Vis Sci.* 2009;50:681–690.
36. Yang H, Sigal IA, Roberts MD, Burgoyne CF, Downs JC. *The Influence of Material Properties and Geometry on Optic Nerve Head Biomechanics*. Presented at the ASME Summer Bioengineering Conference 2009. Lake Tahoe, CA, June 17–21, 2009.
37. Sanfilippo PG, Cardini A, Sigal IA, et al. A geometric morphometric assessment of the optic cup in glaucoma. *Exp Eye Res.* 2010;91; 405–414.
38. Yang H, Downs JC, Bellezza A, Thompson H, Burgoyne CF. 3D histomorphometry of the normal and early glaucomatous monkey optic nerve head: prelaminar neural tissues and cupping. *Invest Ophthalmol Vis Sci.* 2007;48:5068–5084.
39. Sigal IA, Flanagan JG, Tertinegg I, Ethier CR. Modeling individual-specific human optic nerve head biomechanics, II: influence of material properties. *Biomech Model Mechanobiol.* 2009;8:99–109.
40. Downs JC, Suh JK, Thomas KA, Bellezza AJ, Hart RT, Burgoyne CF. Viscoelastic material properties of the peripapillary sclera in normal and early-glaucoma monkey eyes. *Invest Ophthalmol Vis Sci.* 2005;46:540–546.
41. Girard MJ, Downs JC, Bottlang M, Burgoyne CF, Suh JK. Peripapillary and posterior scleral mechanics, II: experimental and inverse finite element characterization. *J Biomech Eng.* 2009;131:051012.
42. Girard MJ, Suh JK, Bottlang M, Burgoyne CF, Downs JC. Scleral biomechanics in the aging monkey eye. *Invest Ophthalmol Vis Sci.* 2009;50:5226–5237.
43. Sigal IA, Hardisty MR, Whyne CM. Mesh-morphing algorithms for specimen-specific finite element modeling. *J Biomech.* 2008;41: 1381–1389.
44. Sander EA, Downs JC, Hart RT, Burgoyne CF, Nauman EA. A cellular solid model of the lamina cribrosa: mechanical dependence on morphology. *J Biomech Eng.* 2006;128:879–889.
45. Yan DB, Flanagan JG, Farra T, Trope GE, Ethier CR. Study of regional deformation of the optic nerve head using scanning laser tomography. *Curr Eye Res.* 1998;17:903–916.
46. Norman RE, Flanagan JG, Rausch SM, et al. Dimensions of the human sclera: thickness measurement and regional changes with axial length. *Exp Eye Res.* 2010;90:277–284.
47. Sigal IA, Roberts MD, Girard M, Burgoyne CF, Downs JC. Biomechanical changes of the optic disc. In: Levin LA, Albert DM eds. *Ocular Disease: Mechanisms and Management*. New York: Elsevier. In press.
48. Burgoyne CF, Downs JC. Premise and prediction: how optic nerve head biomechanics underlies the susceptibility and clinical behavior of the aged optic nerve head. *J Glaucoma.* 2008;17:318–328.
49. Bellezza AJ, Rintalan CJ, Thompson HW, Downs JC, Hart RT, Burgoyne CF. Anterior scleral canal geometry in pressurised (IOP 10) and non-pressurised (IOP 0) normal monkey eyes. *Br J Ophthalmol.* 2003;87:1284–1290.
50. Bellezza AJ, Rintalan CJ, Thompson HW, Downs JC, Hart RT, Burgoyne CF. Deformation of the lamina cribrosa and anterior scleral canal wall in early experimental glaucoma. *Invest Ophthalmol Vis Sci.* 2003;44:623–637.
51. Inoue R, Hangai M, Kotera Y, et al. Three-dimensional high-speed optical coherence tomography imaging of lamina cribrosa in glaucoma. *Ophthalmology.* 2009;116:214–222.
52. Srinivasan VJ, Adler DC, Chen Y, et al. Ultrahigh-speed optical coherence tomography for three-dimensional and en face imaging of the retina and optic nerve head. *Invest Ophthalmol Vis Sci.* 2008;49:5103–5110.
53. Kagemann L, Ishikawa H, Wollstein G, et al. Ultrahigh-resolution spectral domain optical coherence tomography imaging of the lamina cribrosa. *Ophthalmic Surg Lasers Imaging.* 2008;39:S126–S131.
54. Strouthidis NG, Yang H, Fortune B, Downs JC, Burgoyne CF. Detection of optic nerve head neural canal opening within histomorphometric and spectral domain optical coherence tomography data sets. *Invest Ophthalmol Vis Sci.* 2009;50:214–223.
55. Wang JH, Thampatty BP. An introductory review of cell mechanobiology. *Biomech Model Mechanobiol.* 2006;5:1–16.
56. Humphrey JD. Stress, strain, and mechanotransduction in cells. *J Biomech Eng.* 2001;123:638–641.
57. Liang Y, Fortune B, Cull G, Cioffi GA, Wang L. Quantification of dynamic blood flow autoregulation in optic nerve head of rhesus monkeys. *Exp Eye Res.* 2010;90:203–209.
58. Grytz R, Meschke G. Constitutive modeling of crimped collagen fibrils in soft tissues. *J Mech Behav Biomed Mater.* 2009;2:522–533.
59. Mortazavi AM, Simon BR, Stamer WD, Vande Geest JP. Drained secant modulus for human and porcine peripapillary sclera using unconfined compression testing. *Exp Eye Res.* 2009;89:892–897.
60. Brown DJ, Morishige N, Neekhra A, Minckler DS, Jester JV. Application of second harmonic imaging microscopy to assess structural changes in optic nerve head structure ex vivo. *J Biomed Opt.* 2007;12:024029.
61. Ren R, Jonas JB, Tian G, et al. Cerebrospinal fluid pressure in glaucoma: a prospective study. *Ophthalmology.* 2010;117:259–266.
62. Berdahl JP, Allingham RR, Johnson DH. Cerebrospinal fluid pressure is decreased in primary open-angle glaucoma. *Ophthalmology.* 2008;115:763–768.
63. Morgan WH, Yu DY, Cooper RL, Alder VA, Cringle SJ, Constable IJ. The influence of cerebrospinal fluid pressure on the lamina cribrosa tissue pressure gradient. *Invest Ophthalmol Vis Sci.* 1995; 36:1163–1172.
64. Balaratnasingam C, Morgan WH, Johnstone V, Pandav SS, Cringle SJ, Yu DY. Histomorphometric measurements in human and dog optic nerve and an estimation of optic nerve pressure gradients in human. *Exp Eye Res.* 2009;89:618–628.
65. Sigal IA, Flanagan JG, Tertinegg I, Ethier CR. Reconstruction of human optic nerve heads for finite element modeling. *Technol Health Care.* 2005;13:313–329.
66. Downs JC, Blidner RA, Bellezza AJ, Thompson HW, Hart RT, Burgoyne CF. Peripapillary scleral thickness in perfusion-fixed normal monkey eyes. *Invest Ophthalmol Vis Sci.* 2002;43:2229–2235.
67. Olsen TW, Sanderson S, Feng X, Hubbard WC. Porcine sclera: thickness and surface area. *Invest Ophthalmol Vis Sci.* 2002;43: 2529–2532.
68. Jonas JB, Berenshtein E, Holbach L. Lamina cribrosa thickness and spatial relationships between intraocular space and cerebrospinal fluid space in highly myopic eyes. *Invest Ophthalmol Vis Sci.* 2004;45:2660–2665.
69. McBrien NA, Gentle A. Role of the sclera in the development and pathological complications of myopia. *Prog Retin Eye Res.* 2003; 22:307–338.